AD-A181 469 PULSED POWER EQUIPMENT FOR UNIVERSITY ACCELERATOR TECHNOLOGY PROGRAM(U) NEW MEXICO UNIV ALBUQUERQUE INST FOR ACCELERATOR AND PLASMA B.. S HUMPHRIES 1987 1/1

UNCLASSIFIED AFOSR-TR-87-0740 AFOSR-84-0244 F/G 20/7 NL

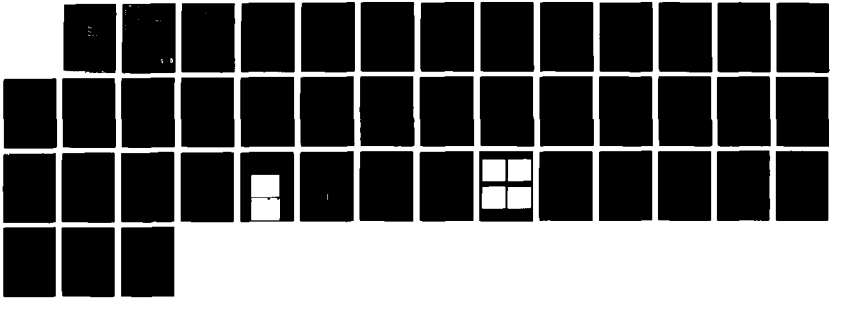

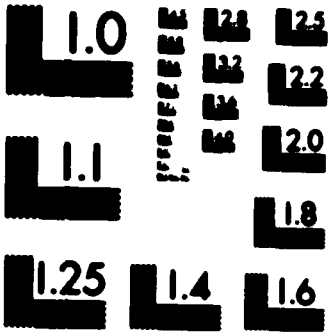

MICROCOPY RESOLUTION TEST CHART
NATIONAL BUREAU OF STANDARDS-1963-A

DTIC FILE COPY

(2)

UNCLASSIFIED

SECURITY CLASSIFICATION OF THIS PAGE

REPORT DOCUMENTATION PAGE

1a. REPORT SECURITY CLASSIFICATION: Unclassified	1b. RESTRICTIVE MARKINGS
2a. SECURITY CLASSIFICATION AUTHORITY	3. DISTRIBUTION/AVAILABILITY OF REPORT: Approved for public release," distribution unlimited
AD-A181 469	5. MONITORING ORGANIZATION REPORT NUMBER(S): AFOSR-TR- 87-0740
6a. NAME OF PERFORMING ORGANIZATION: University of New Mexico; 6b. OFFICE SYMBOL (If applicable):	7a. NAME OF MONITORING ORGANIZATION: AFOSR
6c. ADDRESS (City, State and ZIP Code): University of New Mexico, Department of Electrical & Computer Eng., Albuquerque, New Mexico 87131	7b. ADDRESS (City, State and ZIP Code): Building 410, Bolling AFB, D.C. 20332-6448
8a. NAME OF FUNDING/SPONSORING ORGANIZATION: AFOSR; 8b. OFFICE SYMBOL (If applicable): NP	9. PROCUREMENT INSTRUMENT IDENTIFICATION NUMBER: AFOSR-84-0244
8c. ADDRESS (City, State and ZIP Code): Building 410, Bolling AFB, D.C. 20332-6448	10. SOURCE OF FUNDING NOS.

PROGRAM ELEMENT NO.	PROJECT NO.	TASK NO.	WORK UNIT NO.
61102F	2301	A1	

11. TITLE (Include Security Classification): "PULSED POWER EQUIPMENT FOR UNIVERSITY ACCELERATOR TECHNOLOGY PROGRAM"

12. PERSONAL AUTHOR(S)

13a. TYPE OF REPORT	13b. TIME COVERED	14. DATE OF REPORT (Yr., Mo., Day)	15. PAGE COUNT
FINAL	FROM _____ TO _____		39

16. SUPPLEMENTARY NOTATION

17. COSATI CODES			18. SUBJECT TERMS (Continue on reverse if necessary and identify by block number)
FIELD	GROUP	SUB. GR.	Ferrite, Betatrons, Accelerator

19. ABSTRACT (Continue on reverse if necessary and identify by block number)

Funding from the DOD University Equipment Grant was used to purchase necessary equipment for the construction of a high current betatron experiment. The purchase included ferrite isolation cones, silicon steel isolation cones, HV constant-current power Supplies and HV unregulated power supplies. A paper describing use of this equipment was accepted for publication in Rev. Sci. Intrum.

20. DISTRIBUTION/AVAILABILITY OF ABSTRACT	21. ABSTRACT SECURITY CLASSIFICATION
UNCLASSIFIED/UNLIMITED ☒ SAME AS RPT ☒ OTIC USERS ☐	UNCLASSIFIED

22a. NAME OF RESPONSIBLE INDIVIDUAL	22b. TELEPHONE NUMBER (Include Area Code)	22c. OFFICE SYMBOL
BRUCE L. SMITH	(202)767-4907	NP

DD FORM 1473, 83 APR EDITION OF 1 JAN 73 IS OBSOLETE. UNCLASSIFIED

SECURITY CLASSIFICATION OF THIS PAGE

DISCLAIMER NOTICE

THIS DOCUMENT IS BEST QUALITY PRACTICABLE. THE COPY FURNISHED TO DTIC CONTAINED A SIGNIFICANT NUMBER OF PAGES WHICH DO NOT REPRODUCE LEGIBLY.

FINAL REPORT

DOD UNIVERSITY EQUIPMENT GRANT
CONTRACT NO. AFOSR-84-0244

"Pulsed Power Equipment for University Accelerator Technology Program"

S. Humphries, Jr.
Principal Investigator
Institute for Accelerator and Plasma Beam Technology
Department of Electrical and Computer Engineering
University of New Mexico
Albuquerque, New Mexico 87131

Funding from the DOD University Equipment Grant was used to purchase necessary equipment for the construction of a high current betatron experiment. Betatrons are highly effective electron accelerators. They can produce a high energy beam output with a much smaller volume isolation core than a linear induction accelerator. If the operation of betatrons can be extended to high current, the machines can achieve good net energy efficiency. Betatrons are attractive candidates for military applications requiring compact accelerators and for industrial radiation processing. The UNM Betatron Project has been funded by the Office of Naval Research for the last three years. Funding for an additional 2.5 years has recently been granted.

The following equipment was purchased and incorporated in the Betatron Experiment located in the Nuclear Engineering Laboratory on the UNM campus:

1. Ferrite isolation cores.

   Twenty-five ferrite isolation cores were purchased from TDK. The total cost was $16,855.88. The cores are useful for fast

pulsed induction linacs and magnetic switching. The cores are the same size and material as those used in the Livermore National Laboratory ATA Accelerator. A reprint, included as Appendix 1, describes use of the cores in a magnetically switched injector for the betatron.

2. Silicon steel isolation cores.

Inductive isolation elements are critical for operation of the betatron. The betatron has a long pulselength (10 μs or greater). In order to maximize the volt-second product for a given core size, we ordered silicon steel isolation cores from Arnold Engineering. Ten toroidal cores were purchased; the total cost of the cores and special tooling was $21,718.34. The cores were specially constructed from 4 mil silicon steel to allow investigation of fast betatron cycles. A reprint describing the components of the UNM betatron is included as Appendix 2.

3. High-voltage, Constant-current Power Supplies

The betatron system was designed with the capability of high repetition rate operation. Constant current power supplies were purchased from Glassman High Voltage for fast charging of capacitor banks. Coupled ±60 kV supplies were purchased for the injector and a 30 kV supply was purchased for the main betatron bank. Total cost of the power supplies was $11,757.44.

4. High-voltage, unregulated power supplies

Unregulated 50 kV power packs were purchased from Plastic Capacitors. These supplies are used in the pulsed electrostatic inflector assembly for high energy beam injection into the betatron. Total cost was $1,272.69.

The total money spent on the contract was $51,822.16. The figure includes $217.81 of miscellaneous charges made through the UNM Bureau of Engineering Research. A total of $3,177.84 was returned by UNM at the end of the contract period.

APPENDIX A

Accepted for publication, Rev. Sci. Instrum.

Generation and Propagation of High-brightness Electron Beams from a Magnetically Crowbarred Injector

-S. Humphries, Jr., L.K. Len and C.B. Allen
Institute for Accelerator and Plasma Beam Technology
University of New Mexico
Albuquerque, New Mexico 87131

Abstract

Tests of a 300 keV electrostatic electron beam injector with a magnetic crowbar switch are described. The saturable ferrite core switch allows generation of a constant voltage, 80 ns pulse directly from a Marx generator. Inductive isolation in the switch permits direct access to the high voltage electrode for thermionic or active plasma cathode experiments. The pulse modulator can drive a 1.5 kA load. A high brightness 290 A beam from a felt plasma-emission cathode was extracted and propagated in vacuum. Because of the reliability of the magnetic crowbar switch, more than 500 shots were accumulated on the cathode at over 1 kA/cm^2 with no degradation of the output. The output beam had a normalized brightness of 2.6×10^8 A/m^2-steradian. A solenoidal lens was used to match the space charge dominated beam into a 1 m long periodic focusing system with twenty-five reversing solenoidal coils. A beam current of 150 A was successfully transported through the 1.7 cm radius tube.

Generation and Propagation of High-brightness Electron Beams from a Magnetically Crowbarred Injector

-S. Humphries, Jr., L.K. Len and C.B. Allen
Institute for Accelerator and Plasma Beam Technology
University of New Mexico
Albuquerque, New Mexico 87131

1. Introduction

The operation of a 290 A, 300 kV electron beam generator is described in this paper. The device was designed and built as an injector for the UNM High Current Betatron Project [1]. The application requires a short pulse (≤80 ns) with a fast risetime. In future experiments, the beam will be guided into the circular betatron accelerator by a pulsed electrostatic field. The success of beam injection is critically dependent on the reproducibility and flatness of the generator voltage waveform. We decided to use an undermatched, crowbarred Marx generator to drive the electrostatic electron gun since net energy efficiency was not a major concern. The approach lead to a compact system by avoiding the use of an intermediate high voltage transmission line.

Pulse generators driven directly by an impulse generator typically incorporate a triggered high voltage spark gap as a crowbar switch. Our system is novel in its use of a saturable ferrite core crowbar switch. A magnetic crowbar switch has advantages compared to a spark gap.

1. A magnetic switch does not require a synchronized trigger circuit. Operation of a spark gap is often difficult in a

pulsed power environment because of crosstalk with the primary impulse generator trigger. The magnetic switch cannot prefire as long as the cores are reset.

2. A magnetic crowbar switch clamps at the correct time with 100 per cent reliability. This feature eliminates problems of postpulse damage to the electron gun. The magnetic switch allows high-repetition-rate operation with long cathode lifetime. In hundreds of shots, we have observed no discoloration or erosion of the plasma emission cathode surface. The primary switch fault mode occurs if the cores are not reset. In this case, the circuit energy is harmlessly shunted through the leakage circuit.

3. The magnetic switch acts as an inductive isolator, so that there is direct access to the cathode for power and control cables. We plan future experiments on advanced high brightness cathodes with active plasma sources.

4. The present pulser enclosure permits reconfiguration of the magnetic switch as a 2:1 step-up transformer and crowbar, allowing extension of the operating voltage to 600 kV for a 40 ns pulse. In this case, the injector configuration resembles that of an induction accelerator [2,3,4].

The main drawbacks of the magnetic switch are the initial cost of the ferrite cores and the necessity to reset the core stack between shots.

Design details on the modulator, reset circuit, electron gun and extraction optics are given in SECTION 2. Characteristics of the electron gun and the extracted beam are described in SECTION 3. SECTION 4 presents measurements of beam propagation through a solenoidal magnetic lens to match the space-charge dominated beam to transport systems and experiments. Finally, experimental results on the propagation of 150 A beams through a 1 m, twenty-five cell periodic focusing system are described in SECTION 5. In general, results on the propagation of high current beams are in good agreement with paraxial models of vacuum transport.

2. Experimental apparatus

A schematic diagram of the pulsed voltage system of the injector is shown in FIGURE 1. The output of a low inductance Marx generator is directed through a dropping resistor consisting of four parallel 50 Ω carborundum resistors of length 0.3 m. The downstream end of the resistor is connected directly to the electron gun and to the center conductor of the magnetic switch. The resistor absorbs the energy remaining in the Marx generator after closing of the magnetic switch, allowing the voltage on the electron gun to fall.

The magnetic crowbar switch contains twelve electrically isolated toroidal cores of fast accelerator ferrite [5]. The cores are 0.029 m thick with outer and inner diameters of 0.51 m and 0.239 m. The switch center conductor has a large diameter (0.1 m) to minimize the saturated switch inductance. The center conductor carries a number of shielded signal and power cables to

be used in future experiments. A simplified circuit diagram of the pulser and reset circuit is shown in FIGURE 2. To initiate a shot cycle, the cores are reset by directing an inverse current through the switch center conductor. The reset circuit consists of a low voltage electrolytic capacitor with a damping resistor to prevent ringing. The reset circuit is isolated from the main voltage supply by an oil-immersed, mechanical relay. Operation of the circuit is straightforward. When the Marx generator is fired, the magnetic switch presents a high impedance because of the inductance of the cores (~60 μH). After a time interval determined by the generator voltage and the core area, the cores become saturated and the switch inductances drops to a low value (~0.1 μH). Following saturation, most of the generator voltage appears across the dropping resistor.

The electron gun, illustrated in FIGURE 3, consisted of a 1.3 cm diameter field emission cathode and a grid anode. The cathode surface was composed of ordinary felt material fastened to a metal substrate with high vacuum epoxy. We adopted felt because our previous experiments with carbon fibers [6] were disappointing. In common with other experimenters [7,8], we found that felt provided uniform emission, high current density and fast current initiation at relatively low field strengths. The anode consisted of a 0.038 m diameter extraction port covered with fine stainless steel mesh. The electron gun geometry was such that only about 20 per cent of the diode current was extracted. Extraction efficiency does not present experiments since no more than 100

the betatron and a diode current of 1.2 kA provides a good match to the pulse modulator. Furthermore, we found that the extracted portion of the beam had high brightness.

The extracted beam had a net divergence, so a solenoidal magnetic lens (FIGURE 3) was incorporated downstream from the anode to match the beam to different transport systems. We performed vacuum propagation experiments with a 1 meter transport tube, illustrated in FIGURE 4. Twenty-five independent solenoidal coils were wound on the tube. Coil inputs could be modified so that the fields of individual coils were either in the same direction or of alternating polarity. It was therefore possible to make a direct comparison between a periodic magnetic focusing system and an extended solenoidal field. The transport tube was driven by an independent 160 A transistor circuit; the maximum solenoidal field was 0.2 tesla.

The electron gun voltage was measured with a shielded resistive probe attached directly to the gun. Total electron current to the anode was measured by a shielded Rogowski loop. Current in the transport sections was measured with matched shielded Rogowski loops (FIGURE 4) with a 5.4 cm inner diameter. The time-integrated beam profile and emittance were determined by the detector illustrated in FIGURE 4 [9]. The 5.4 cm diameter stainless steel aperture plate had 5×10^{-2} cm diameter holes separated on a square pattern with 0.5 cm center to center. The detector was a glass vacuum plate 1.7 cm from the aperture plate. The Cherenkov light generated by the relativistic electrons was

proportional to the electron current density. The vacuum side of the plate was sprayed with an opaque layer of graphite to relieve charge accumulation. Light emission was recorded by time-integrated photography.

3. Electron Diode Tests

Waveforms of electron gun voltage and net current with an electron beam load at peak Marx generator charge are shown in FIGURE 5. The 1.3 cm diameter cathode was located at a distance of 2 cm from the anode mesh. The net current was about 1.5 kA at a gap voltage of 280 kV. The current density at the cathode exceeded 1 kA/cm^2. Voltage flatness was ±2% over the central 70 ns of the pulse.

Electron flow was initiated in the cathode less than 10 ns after the start of the voltage pulse. The current and voltage were quite reproducible. Note that the current rose slightly over the pulselength. The current enhancement was caused by plasma expansion into the acceleration gap; the effect is more evident at longer pulselength. FIGURE 6 shows a voltage and current trace for a 180 kV open circuit generator voltage. The current increased a factor of 1.8 in 175 ns. The dashed line in FIGURE 6 is a theoretical prediction based on a uniform closure velocity of 3 $cm/\mu s$. Long pulse operation with lower closure velocity has been obtained with felt cathode surfaces [10,11], but at much reduced current density (<100 A/cm^2).

The current and distribution of the extracted beam were

measured with the integrated diagnostic package shown in FIGURE 4. For initial measurements, the package was mounted on the anode holder flange, 5 cm from the anode mesh. The extracted current (FIGURE 7(a)) entering the matching lens had an average value of 290 A, representing 20 per cent of the total diode current flow. A time integrated photograph of the emittance box light output is reproduced in FIGURE 7(b) along with a reference photograph (FIGURE 7(c)). The aperture pattern at the center of the plate was drilled on a fine scale to identify the center and to resolve details of focused beams. There was some structure in the central spots, possibly representing cathode emission non-uniformities. Despite this, the brightness of the extracted beam was excellent [12]. FIGURE 8(a) shows a boundary beam distribution, $f(x,x')$, derived from the maximum width of the spots in FIGURE 8(b). The beam had a linear divergence. The effective beam radius was 1.7 cm with a 0.16 radian divergence at the envelope. The emittance corresponding to the fitted ellipse of FIGURE 8(a) (dashed line) was $\epsilon = 2.8 \times 10^{-4}$ π-m-rad; the normalized emittance was $\epsilon_n = \beta\gamma\epsilon = 3.3 \times 10^{-4}$ π-m-rad. Combining the measured emittance and current, the normalized brightness was

$$B_n = I/(\pi\epsilon_n)^2 = 2.7 \times 10^8 \text{ A/(m}^2\text{-steradian)}. \qquad (1)$$

The brightness figure is comparatively high, within the range required for free electron laser experiments.

4 Matching Lens Experiments

The solenoidal lens downstream from the anode matched the

diverging beam to the betatron transport tube and other experiments. The lens, illustrated in FIGURE 3, consisted of two solenoidal windings mounted on a vacuum tee. The free arms of the tee were used for extractable beam diagnostics. The measured magnetic field profile was used to generate numerical predictions of the beam envelope over the length of the lens using a paraxial equation with space charge and beam emittance included [13]. FIGURE 9 (a)-(e) shows the envelope trace as a function of lens current. The calculation assumed a 1.5 cm envelope radius, a beam current of 265 A, and an initial envelope divergence of 0.16 at the position of the extracted beam measurements of SECTION 3. The dashed line shows the position of the downstream detector assembly.

As expected from FIGURE 9, beam current transported to the downstream detector reached a maximum value at a lens current of about 80 A. The peak detected current was 265 A implying a transport efficiency exceeded 90%. FIGURE 10 shows a summary of transported current versus lens current for two values of the Marx charging voltage, corresponding to beam energies of 283 keV and 225 keV. The peak current was reduced at lower charge voltage because of space charge effects in the gun. The effect of the decrease in lens focal length at the lower energy is evident in the shift of the optimum lens current. Although there is qualitative agreement between the measurement of FIGURE 10 and the predictions of FIGURE 9, there are quantitative discrepancies. The calculations predict that if the beam has a well-defined envelope, the full beam current will be accepted by

the detector at all values of lens current above 50 A. The measurements imply that the beam has a substantial halo. This is consistent with the extracted beam distribution measurements which indicate that the beam does not have uniform density with radius. In consequence, space charge forces acting on the beam during propagation through the 24 cm lens assembly are non-linear.

Photographs of the beam distribution at the lens exit for different values of lens current are shown in FIGURE 11. The beam radius was close to the predictions of FIGURE 9 considering possible errors in fixing the lens current, beam current, magnetic field distribution, and entrance beam parameters. The beam distribution at 52.5 A (FIGURE 11(a)) had an envelope radius of about 2 cm and a convergence angle of -47 mrad; at 65.6 A (FIGURE 11(b)), the radius was reduced to 1.25 cm with a -112 mrad convergence angle. As expected, the minimum beam radius (0.9 cm) and convergence angle (14 mrad) occurred at a coil current of 79 A (FIGURE 11(c)). In this case, the high flux of the focused beam focus caused some spurious light production in the glass detector, probably the result of space charge discharges. With a lens current of 91.9 A (FIGURE 11(d)), a halo of expanding electrons was visible in the photograph. The density distribution of the compressed beam had good azimuthal symmetry but was clearly non-uniform in the radial direction. Because of the action of non-linear space charge forces at the convergence point, it was impossible to identify an envelope convergence angle for lens currents above 80

A. In general, we concluded that beam propagation in high vacuum through the lens up to the point of maximum convergence was well-described by a paraxial envelope model and that optimum matching to a downstream transport system should be achieved at a lens current of about 80 A.

5. Beam transport experiments

The 1 meter long, 1.7 cm radius transport tube described in SECTION 2 is intended to carry the electron beam from the injector into the circular betatron accelerator. The tube also will provide vacuum isolation to prevent gas and plasma generated in the electron gun from contaminating the high vacuum environment environment of the betatron. At an injection voltage of 280 kV, the maximum current that can be contained in the betatron at high vacuum is about 100 A. The transport tube has 25 individual solenoidal coils that are driven in series, either with the same or alternating field polarity. We are particularly interested in transport of space charge dominated beams in the reversing solenoidal lens configuration since the focusing geometry will be used in the betatron.

The experimental apparatus is illustrated in FIGURE 4. The current monitor and emittance box were attached at the downstream end of the tube. A matching large diameter current monitor measured the total arriving at the entrance flange to the transport tube. At maximum charge, the coil driving circuit supplied 108 A, corresponding to a peak field of $B_z = 1.1 \times 10^{-2}$ tesla. The field variation in the reversing solenoid array was

almost harmonic. The focusing effect of the field can be approximated by a continuous field of magnitude $B = \langle B_z^2 \rangle = B_o^2/2$ in the limit that the betatron wavelength is long compared to the cell size. In this case, the betatron wavelength is approximately

$$\lambda_b \cong \sqrt{8}\pi\gamma\beta m_e c/qB_o. \qquad (2)$$

The betatron wavelength is 57 cm for 283 keV electrons, much greater than the 3.9 cm cell length. Neglecting emittance, the beam self-forces in the transport tube are balanced by the magnetic focusing force if

$$B_o^2 = 4m_e I_b/qr_b^2\pi\epsilon_o\gamma\beta c, \qquad (3)$$

where I_b is the net beam current and r_b is the beam envelope radius.

Measurements were made of current transported through the 1 m tube as a function of driving current in the matching lens and the transport tube coils. FIGURE 12(a) shows a plot of current at the entrance flange of the transport tube and at the far end of the tube as a function of matching lens current for tube coil current at the maximum value of 108 A. As expected from beam distribution measurements at the tube entrance and orbit predictions, capture and transport through the tube was best near the matched beam condition (minimum radius and envelope inclination). At a lens coil current of 68.3 A, about one half the available current was captured and carried through the transport tube. The capture efficiency was consistent with the observed entrance beam distribution with its substantial halo.

Note that the current captured in the tube was quite sensitive to the setting of lens field as expected from an inspection of FIGURE 9. The peak transported current was 150 A. The distribution of the beam emerging from the transport tube is plotted in FIGURE 8(b). The output beam had a RMS radius of about 1 cm. The emittance was 9.4×10^{-4} π-m-rad. The factor of three emittance dilution (compared to the distribution near the gun) was the cumulative result of focusing by the matching lens and passage through the 1 m tube.

FIGURE 12(b) shows transported beam current as a function of the transport tube coil current for both reversing and straight solenoidal field configurations. For the reversing field case, EQUATION 3 predicts that B_o must be greater than or equal to 0.061 tesla for radial equilibrium of a beam with T_e = 283 keV, r_b = 1 cm and I_b = 150 A. This field corresponds to a tube current of 93 A. The tube current required for complete current transport is somewhat larger; the discrepancy is probably the result of emittance and possible mismatch. In comparing the straight solenoidal field to the reversing geometry, note that the maximum value of transported beam current is the same for both case. The straight solenoid requires lower tube current to reach the maximum level. This reflects the fact that the quantity $\langle B_z^2 \rangle$ for the straight solenoid is higher for a given tube current. Magnetic field measurements showed that the mean square axial field for the straight solenoid was a factor of 4 [illegible] higher than that for the reversing geometry. This [illegible] the alternating polarity configuration requires about [illegible]

drive current to achieve the same focusing strength. With sufficient drive current, we observed no significant changes in the transport efficiency or the distribution of the emerging beam with the coil polarity.

In conclusion, the magnetically crowbarred injector with felt surface cathode has proved to be a reliable electron beam generator. The high repetition rate capability permitted detailed studies of beam transport. The space charge dominated output beam was propagated through an extended transport system. The first order behavior of the beam was well described by paraxial vacuum transport theory. The available output beam current of 150 A exceeds the requirements for near-term betatron experiments.

This work was supported by the Office of Naval Research under Contract No. N00014-84K-0248. We would like to thank D. Moir of Los Alamos National Laboratory for suggestions on the emittance diagnostic and the HIFAR Group of the Lawrence Berkeley Laboratory for the loan of switch ferrites.

REFERENCES

1. S. Humphries, Jr. and D.M. Woodall, Bull. Am. Phys. Soc. 28, 1054 (1983).

2. N.C. Christofilos, Rev. Sci. Instrum. 35, 886 (1964).

3. R. Avery, G. Behrsing, W.W. Chupp, A. Faltens, E.C. Hartwig, H.P. Hernandez, C. Macdonald, J.R. Meneghetti, R.G. Nemetz, W. Popenuck, W. Salsig, and D. Vanacec, IEEE Trans. Nucl. Sci. NS-18, 479 (1971).

4. See, for instance, J. Leiss, IEEE Trans. Nucl. Sci. NS-26, 3870 (1979).

5. TDK type P11B .

6. K.W. Zieher, B. Fishbine, S. Humphries, Jr., and D.M. Woodall, IEEE Trans. Nucl. Sci. NS-32, 3274 (1985).

7. R.J. Adler, G.F. Kiuttu, B.E. Simpkins, D.J. Sullivan, and D.E. Voss, "Improved Electron Emission by Use of a Cloth Fiber Cathode," AMRC-N-275 (1984), unpublished.

8. J.T. Weir, G.J. Caporaso, F.W. Chambers, R. Kalibjian, J Kallman, D.S. Prono, M.E. Slominsky, and A.T. Paul, IEEE Trans. Nucl. Sci. NS-32, 1812 (1985).

9. J.C. Elliot, R.J. Faehl, H.J. Fullbright, D.C. Moir, and C.E. Swannack, IEEE Trans. Nucl. Sci. NS-28, 2699 (1981)

10. Private communication, G. Proulx, Pulse Sciences, Inc.

11. R.E. Klinkowstein and R.E. Shefer, Bull. Am. Phys. Soc. 31, 1396 (1986).

12. Definitions of emittance and brightness are reviewed in C. Lejeune and J. Aubert, "Emittance and Brightness: Definitions and Measurements," in Applied Charged Particle Optics, Supplement 13A, edited by A. Septier (Academic Press, New York, 1980).

13. See, for instance, J.D. Lawson, The Physics of Charged Particle Beams (Clarendon, Oxford, 1977).

FIGURE CAPTIONS

1. Scale drawing of pulsed voltage system.

2. Circuit diagram of pulsed power modulator.

3. Scale drawing of electron gun assembly with matching magnetic lens.

4. Transport tube with periodic focusing system showing diagnostics to measure net current, profile and emittance of electron beam.

5. Electron gun voltage and net gap current, direct digitizer output. Marx generator open circuit voltage: 300 kV. 1.3 cm diameter felt cathode, 2 cm gap spacing. Abscissa: 50 ns/div. a) Current 400 A/div. b) Voltage: 70 kV/div.

6. Electron gun traces showing diode closure effect from felt cathode surface. Marx generator open circuit voltage: 180 kV. Abscissa: 50 ns/div. a) Voltage: 70 kV/div. b) Current: 480 A/div. Dashed line is theoretical prediction for closure velocity of 3 cm/μs.

7. Measurements of extracted beam parameters 5 cm from anode mesh. Marx generator open circuit voltage; 300 kV. a) Beam current. Ordinate: 110 A/div. Abscissa: 50 ns/div. b) Time-integrated Cherenkov light output from emittance diagnostic. c) Reference photograph of emittance diagnostic. Width of exposed glass plate: 5.08 cm.

8. Beam boundary distributions. Bars indicate full width of beam spots, circles denote dim spots of same width as apertures, dashed line is a fitted emittance ellipse. Marx open circuit voltage: 300 kV. a) Extracted beam distribution, 5 cm from anode mesh, 290 A. b) Distribution of beam emerging from end of 1 m transport tube, 160 A. Matching lens current, 68.3 A. Tube coil current: 108 A.

9. Numerical predictions of beam radius as a function of axial position and matching lens coil current using paraxial envelope equation. Space charge forces and exact form of lens magnetic field variation included. Left boundary: Position of measurement, FIGURE 11. Entrance conditions: I = 265 A, r_o = 1.5 cm, r_o' = 0.16 rad. Dashed line: Position of measurements, FIGURES 15 and 16.

10. Beam current collected within a 2.6 cm radius at the downstream end of the lens assembly as a function of lens coil current. Circles: Marx generator open circuit voltage: 240 kV. Squares: Marx generator open circuit voltage: 300 kV.

11. Time-integrated emittance diagnostic output at downstream end of lens assembly as a function of lens current. a) 52.5 A. b) 65.6 A. c) 78.8 A. d) 91.9 A.

12. Experiments with 25 cell periodic focusing system. a) Beam current transported as a function of matching lens current for transport coil current of 108 A. Alternating polarity cells. Squares: Total beam current at entrance flange of 1 m transport tube. Circles: Current emerging from transport tube. b) Beam current as a function of transport coil current for a matching lens current of 68.3 A. Circles: Current emerging from transport tube with all cell coils, same polarity. Squares: Cell coils with alternate polarity.

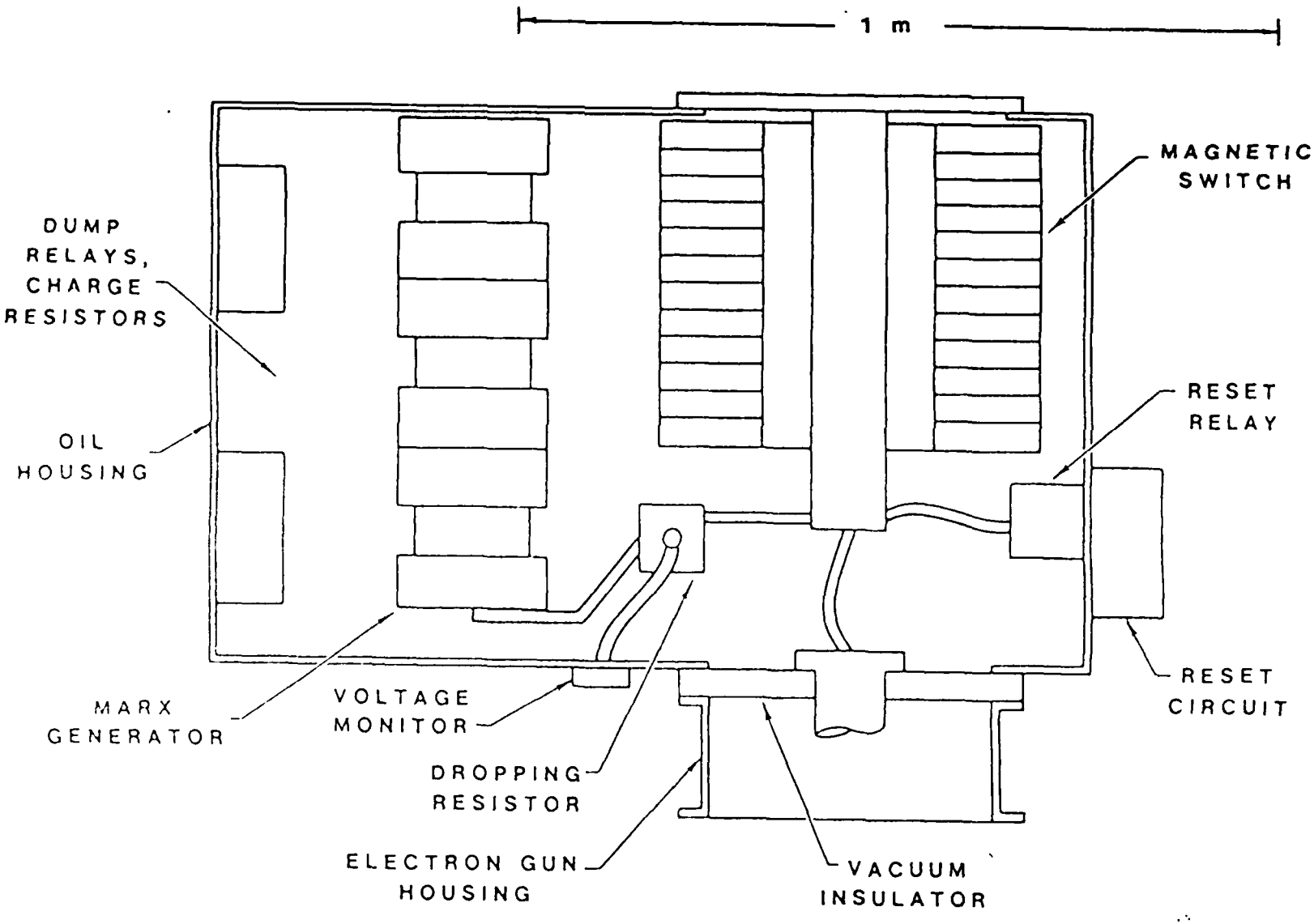
1 m
MAGNETIC SWITCH
DUMP RELAYS, CHARGE RESISTORS
OIL HOUSING
RESET RELAY
MARX GENERATOR
VOLTAGE MONITOR
DROPPING RESISTOR
RESET CIRCUIT
ELECTRON GUN HOUSING
VACUUM INSULATOR

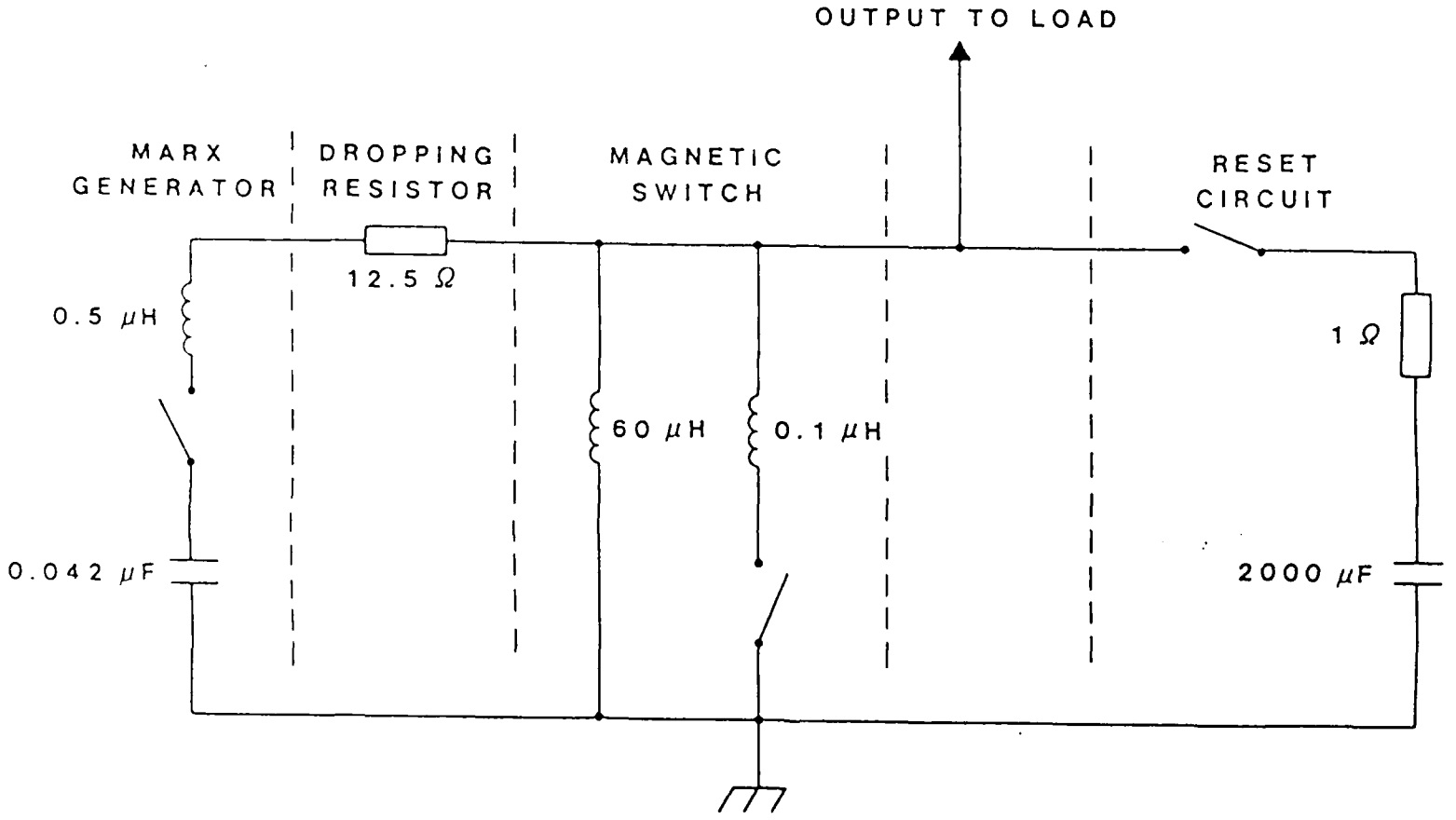
OUTPUT TO LOAD
MARX GENERATOR
DROPPING RESISTOR
MAGNETIC SWITCH
RESET CIRCUIT
12.5 Ω
0.5 μH
1 Ω
60 μH
0.1 μH
0.042 μF
2000 μF

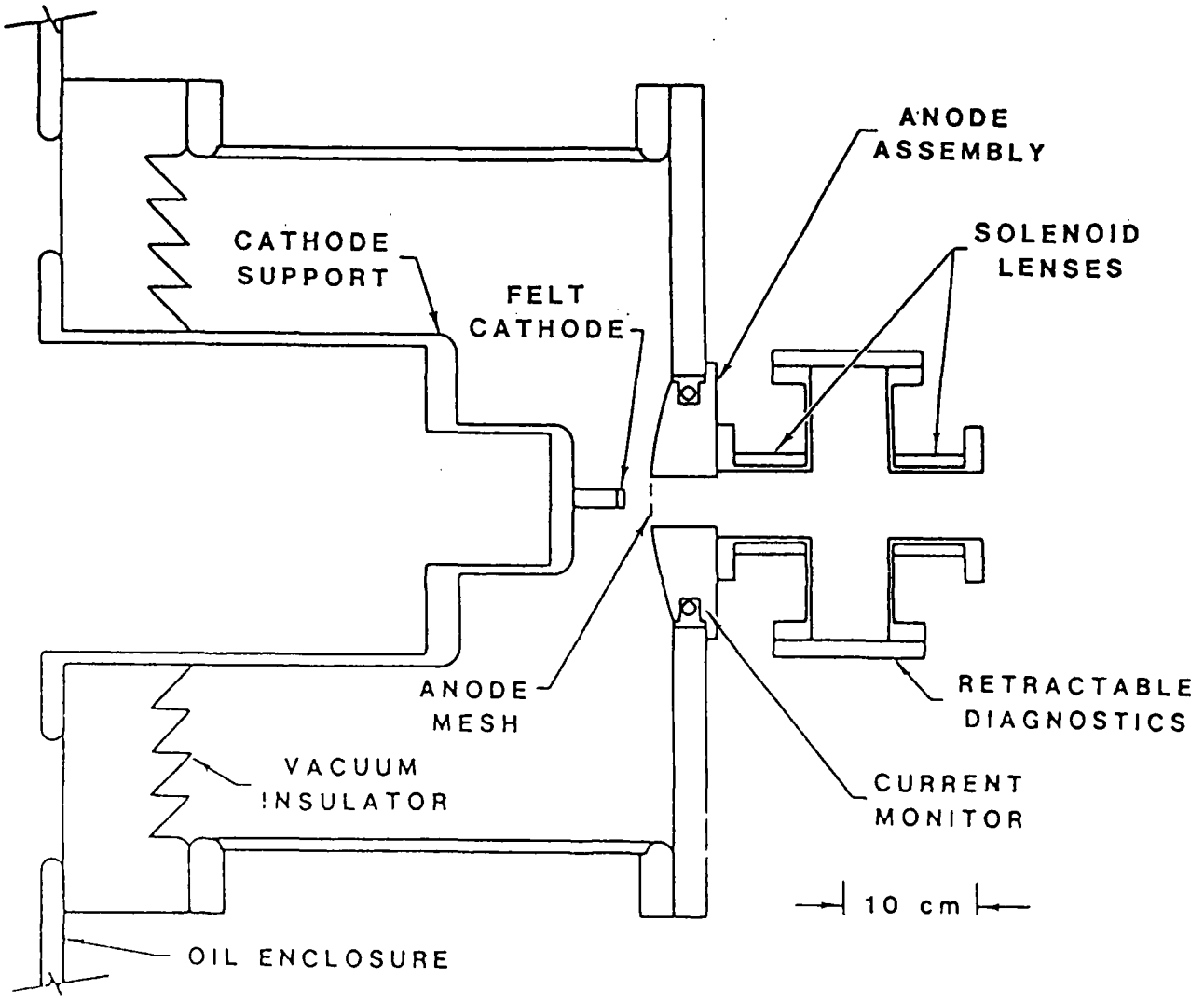
ANODE
ASSEMBLY
SOLENOID
LENSES
CATHODE
SUPPORT
FELT
CATHODE
ANODE
MESH
RETRACTABLE
DIAGNOSTICS
VACUUM
INSULATOR
CURRENT
MONITOR
10 cm
OIL ENCLOSURE

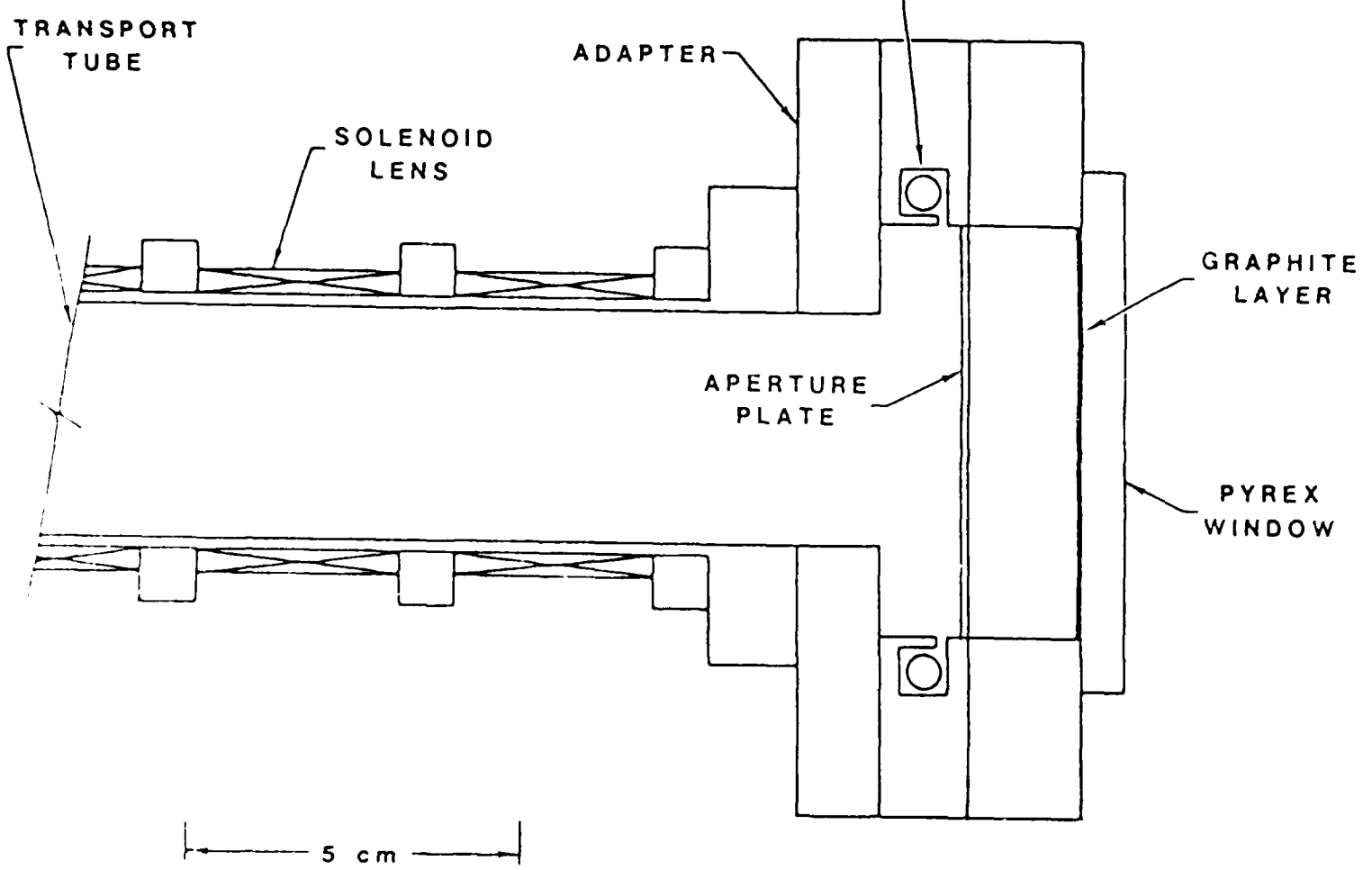
SHIELDED
ROGOWSKI
LOOP
TRANSPORT
TUBE
ADAPTER
SOLENOID
LENS
GRAPHITE
LAYER
APERTURE
PLATE
PYREX
WINDOW
5 cm

a)

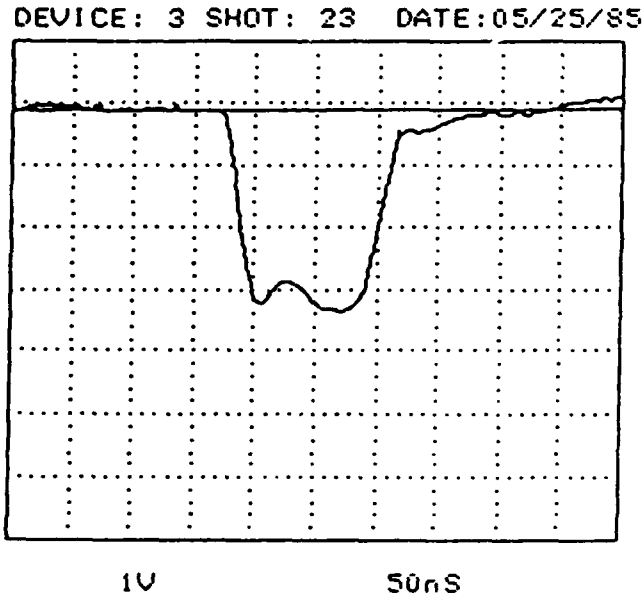
DEVICE: 3 SHOT: 23 DATE:05/25/85
1V
50nS

b)

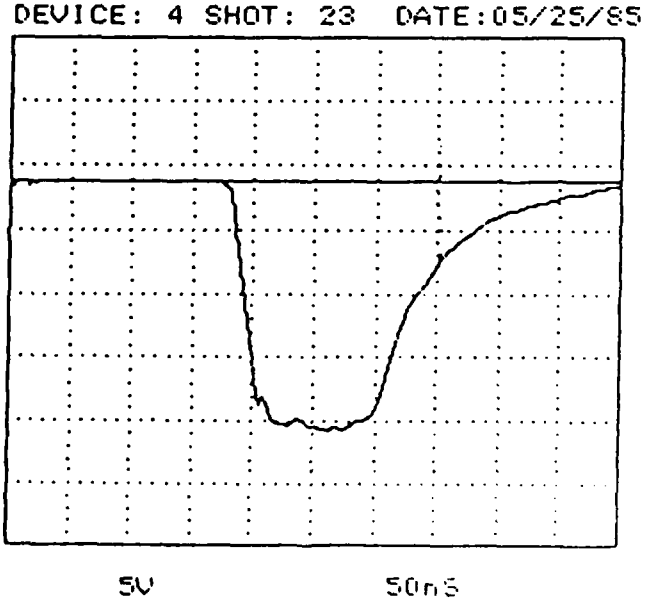
DEVICE: 4 SHOT: 23 DATE:05/25/85
5V
50nS

a)

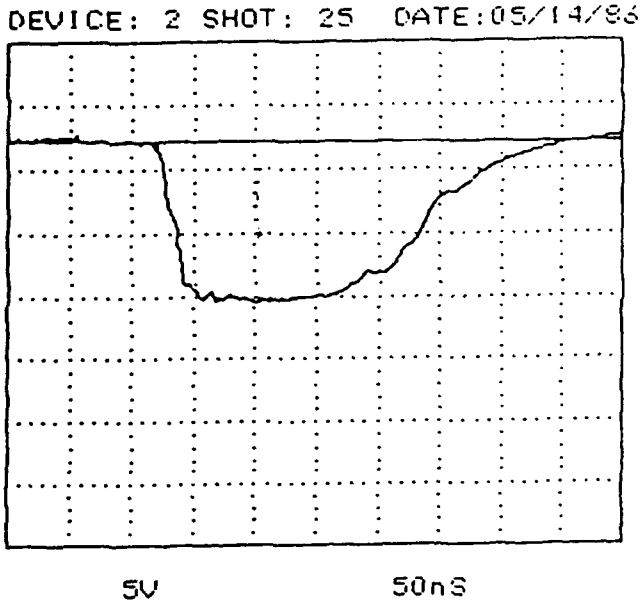
DEVICE: 2 SHOT: 25 DATE:05/14/86
5V
50nS

b)

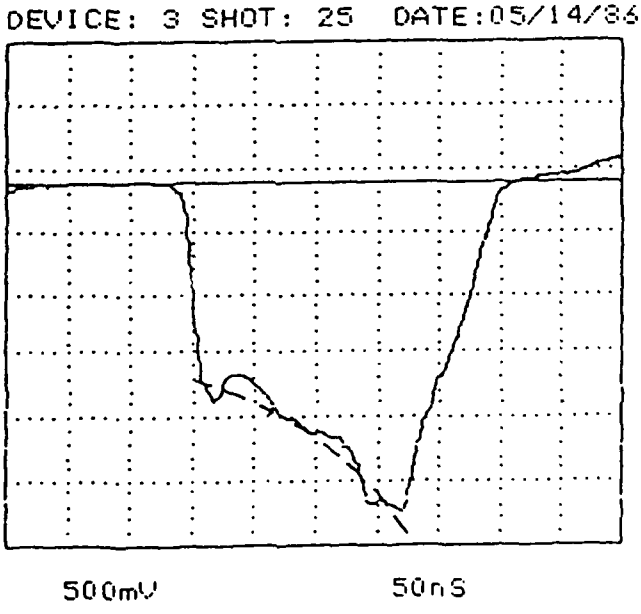
DEVICE: 3 SHOT: 25 DATE:05/14/86
500mV
50nS

a)

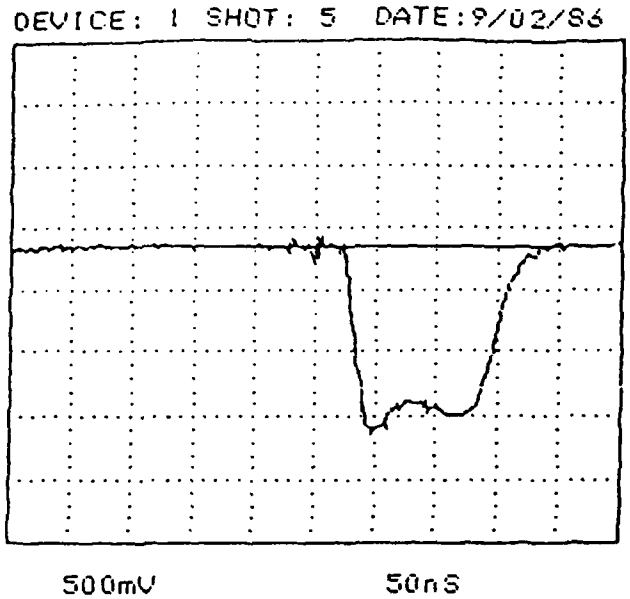

b)

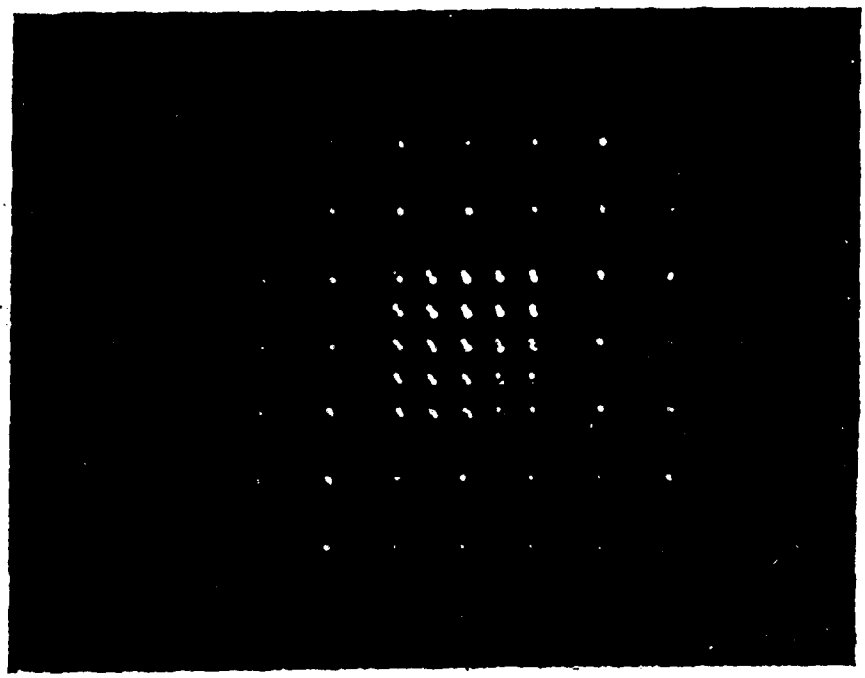

c)

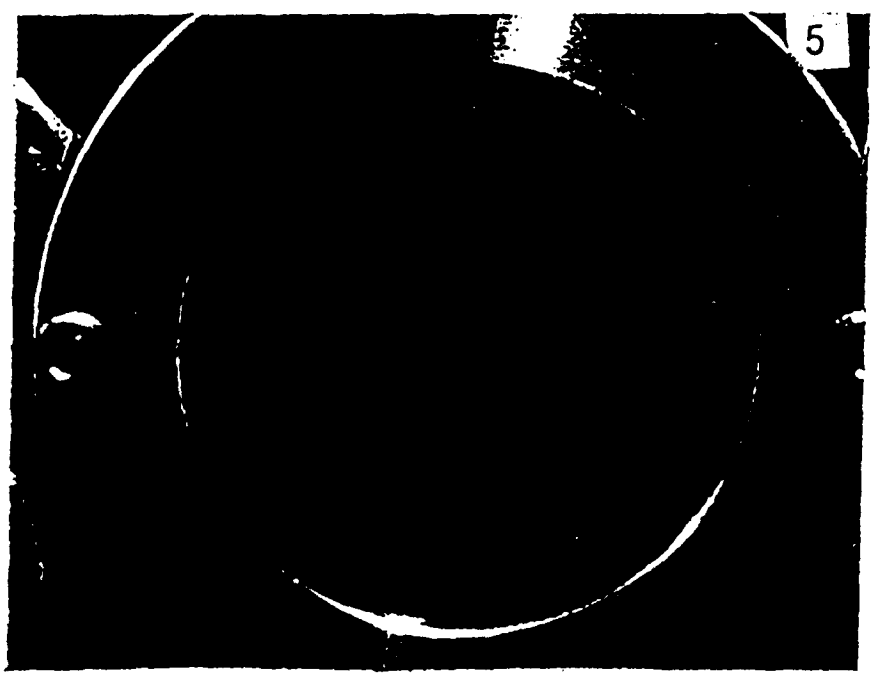

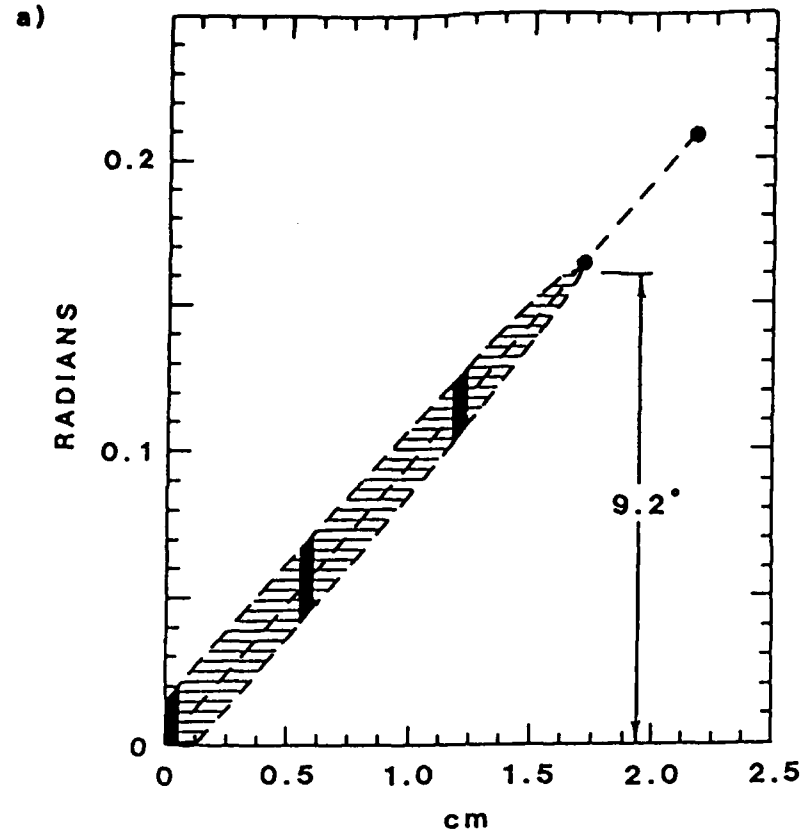
a)
0.2
0.1
0
RADIANS
9.2°
0
0.5
1.0
1.5
2.0
2.5
cm

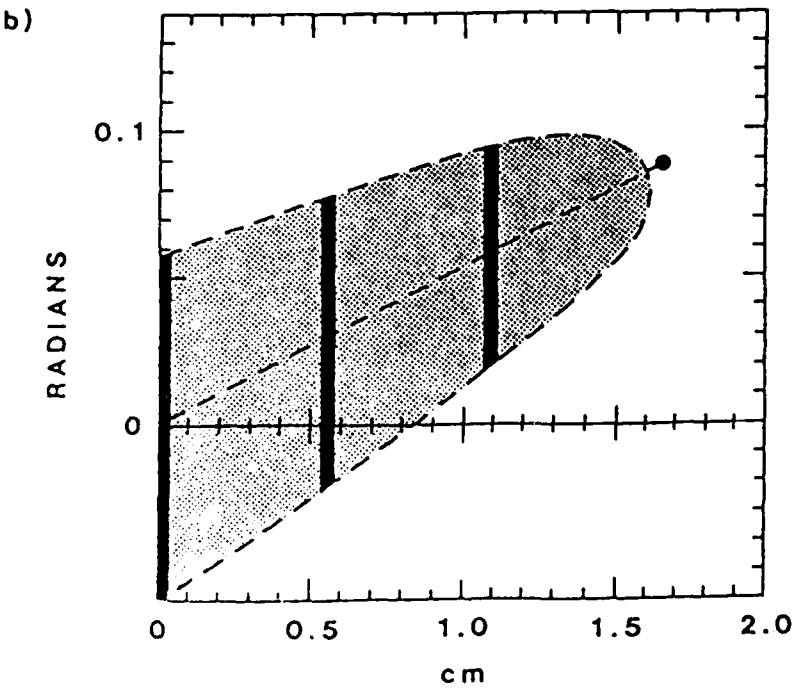
b)
0.1
0
RADIANS
0
0.5
1.0
1.5
2.0
cm

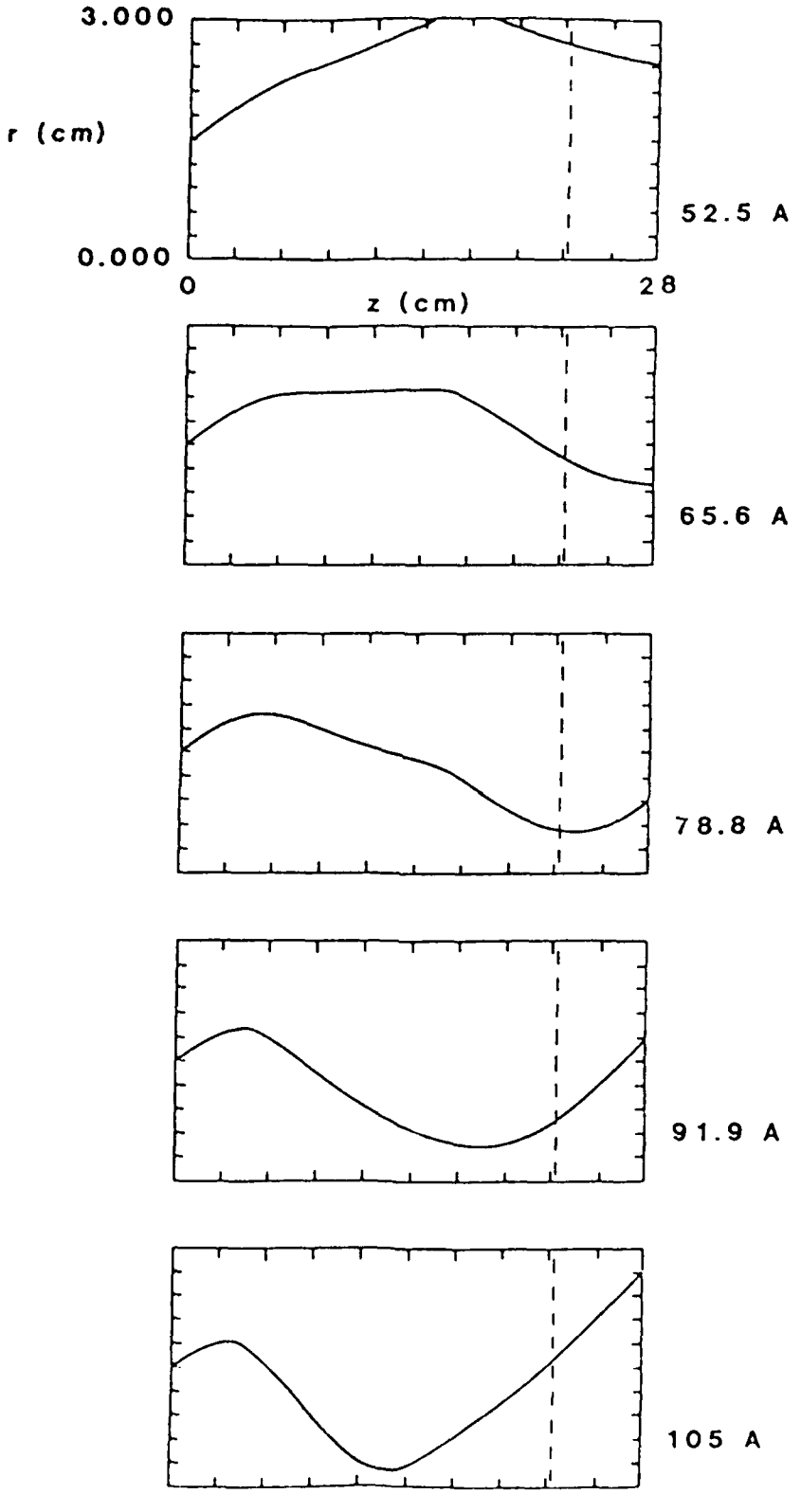
3.000
r (cm)
0.000
0
28
z (cm)
52.5 A
65.6 A
78.8 A
91.9 A
105 A

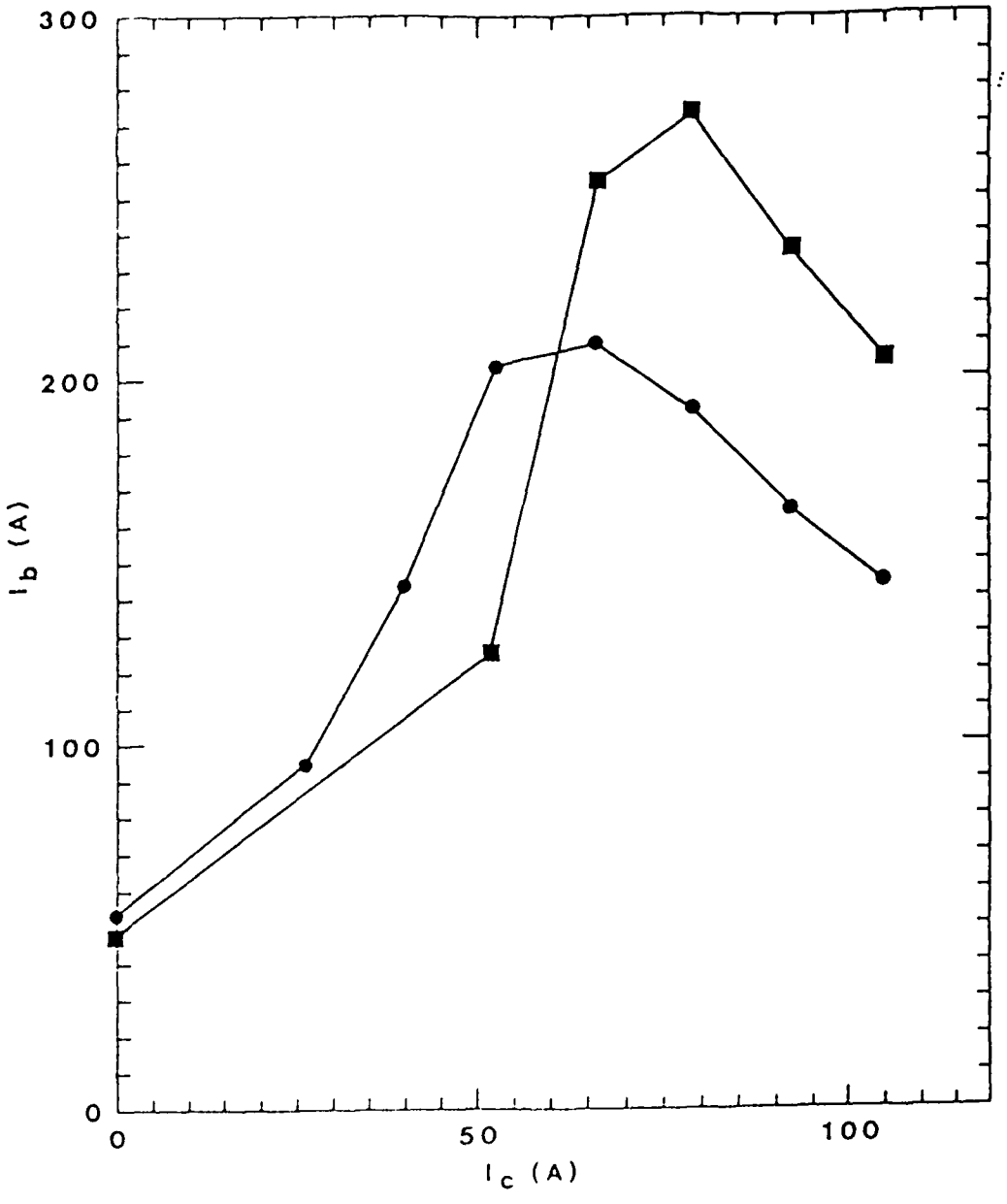
300
200
100
0
0
50
100
I_b (A)
I_c (A)

a)

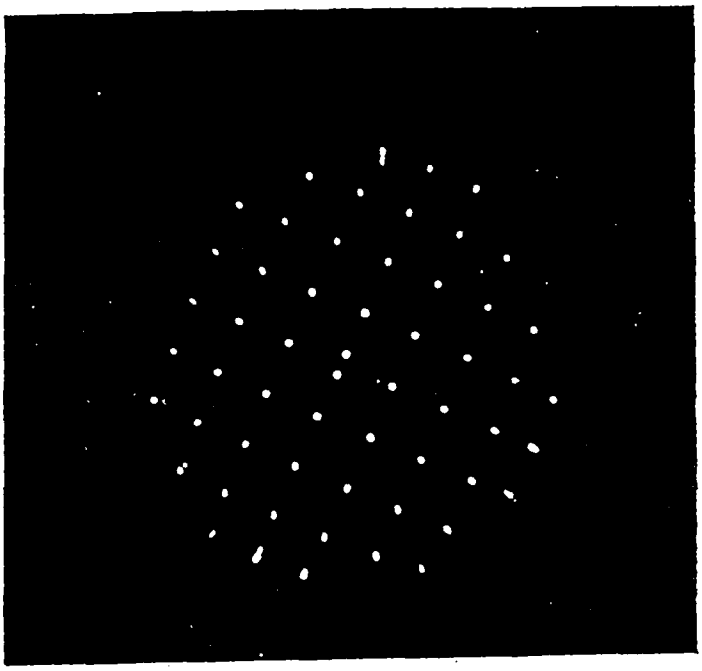

b)

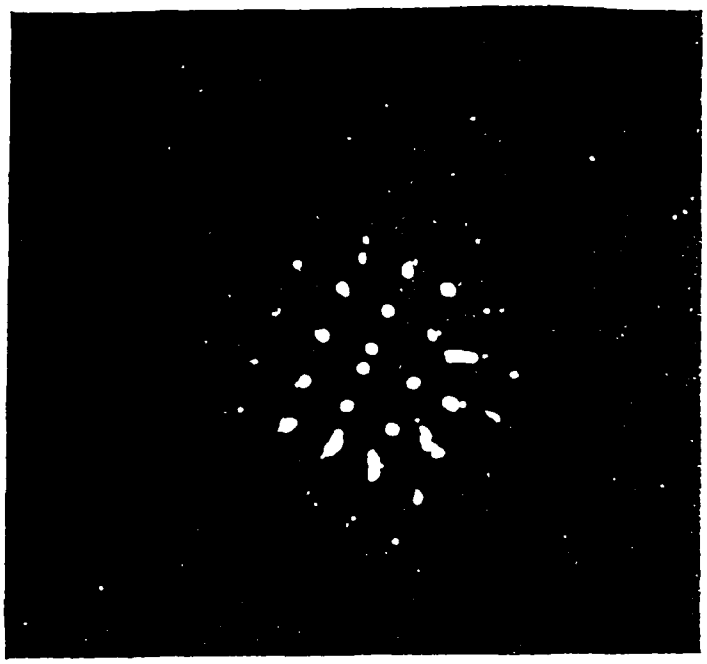

c)

d)

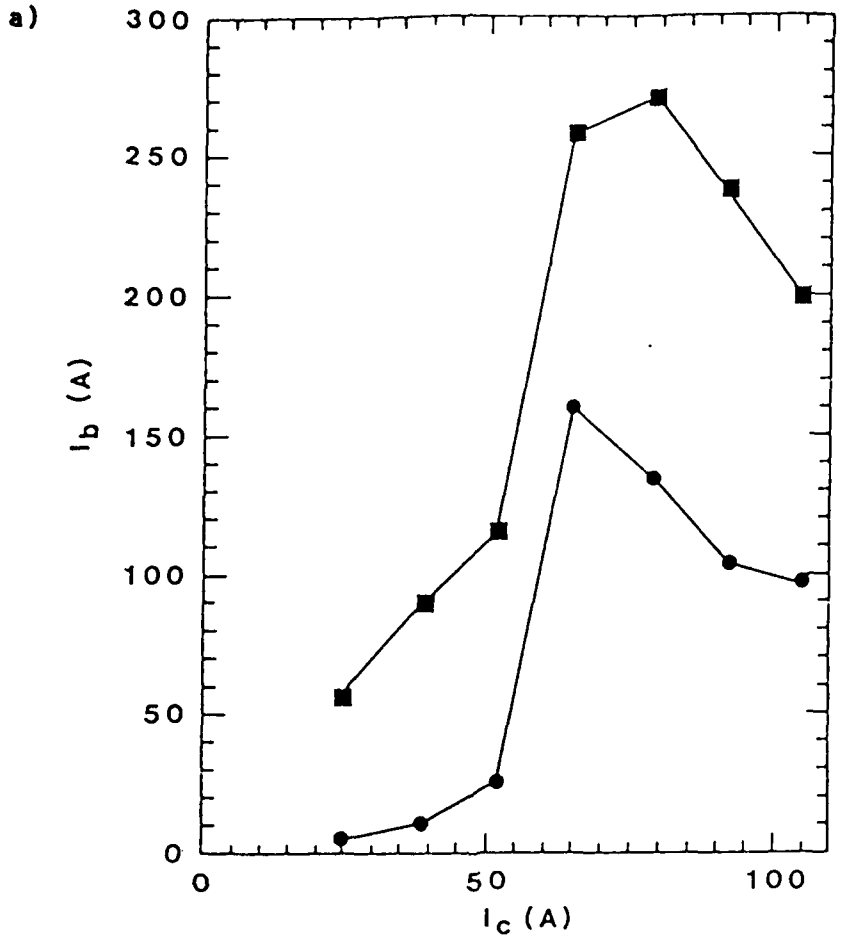
a)
300
250
200
150
100
50
0
I_b (A)
0
50
100
I_c (A)

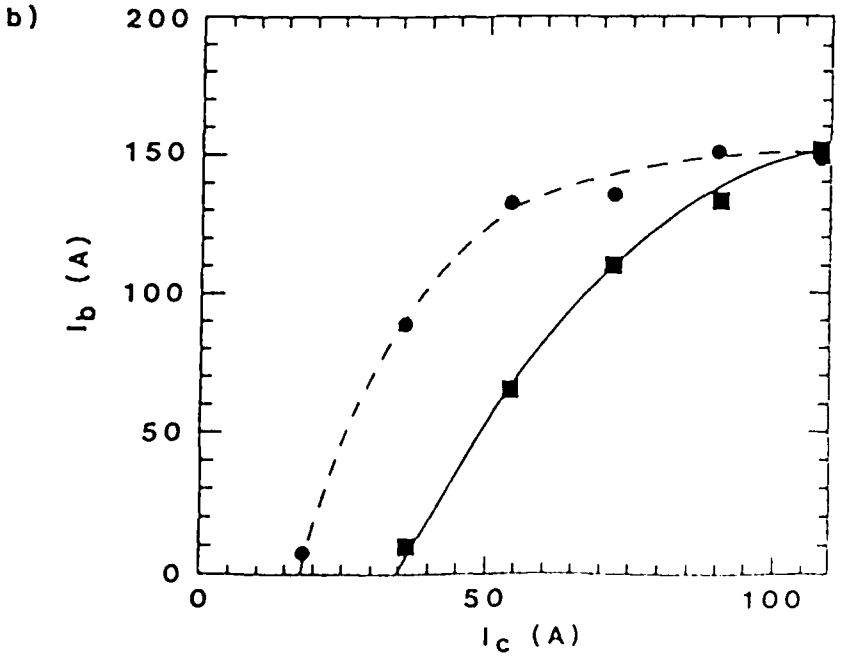
b)
200
150
100
50
0
I_b (A)
0
50
100
I_c (A)

APPENDIX B

HIGH CURRENT BETATRON RESEARCH AT THE UNIVERSITY OF NEW MEXICO

-S. Humphries, Jr. and L.K. Len
Institute for Accelerator and
Plasma Beam Technology
University of New Mexico
Albuquerque, New Mexico 87131

Proceedings of the 1987
Particle Accelerator Conference

HIGH CURRENT BETATRON RESEARCH AT THE UNIVERSITY OF NEW MEXICO

S. Humphries, Jr. and L.K. Len
Institute for Accelerator and Plasma Beam Technology
University of New Mexico
Albuquerque, New Mexico 87131

1. Introduction

Betatrons are among the simplest of high energy accelerators. Their circuit is equivalent to a step-up transformer; the electron beam forms a multi-turn secondary winding. Circulation of the beam around the flux core allows generation of high energy electrons with relatively small core mass. As with any transformer, a betatron is energy inefficient at low beam current; the energy balance is dominated by core losses. This fact has prompted a continuing investigation of high current betatrons as efficient, compact sources of beta and gamma radiation [1].

A program has been supported at the University of New Mexico by the Office of Naval Research to study the physics of high current electron beams in circular accelerators and to develop practical technology for high power betatrons [2]. Fabrication and assembly of the main ring was completed in January of this year. In contrast to other recent high current betatron experiments [3,4] the UNM device utilizes a periodic focusing system to contain high current beams during the low energy phase of the acceleration cycle. The reversing cusp fields generated by alternating polarity solenoidal lenses cancel beam drift motions induced by machine errors. In consequence, we have found that the cusp geometry has has significantly better stability properties than a monodirectional toroidal field. In comparison to other minimum-B geometries such as the Stellatron [5], cusps have open field lines which facilitate beam injection and neutralization.

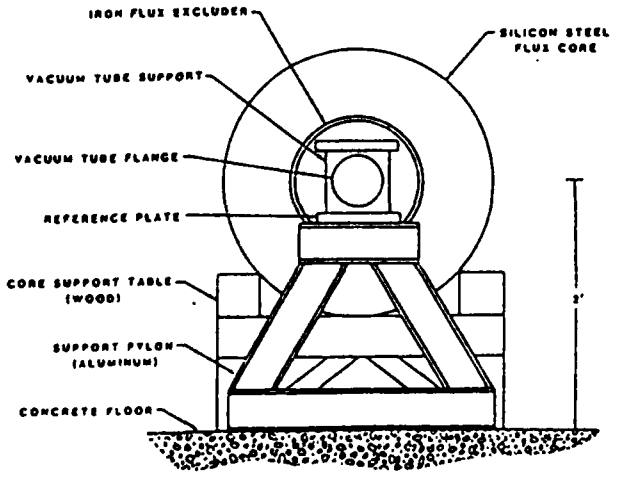

Fig. 1. Cross section of main ring, UNM Betatron.

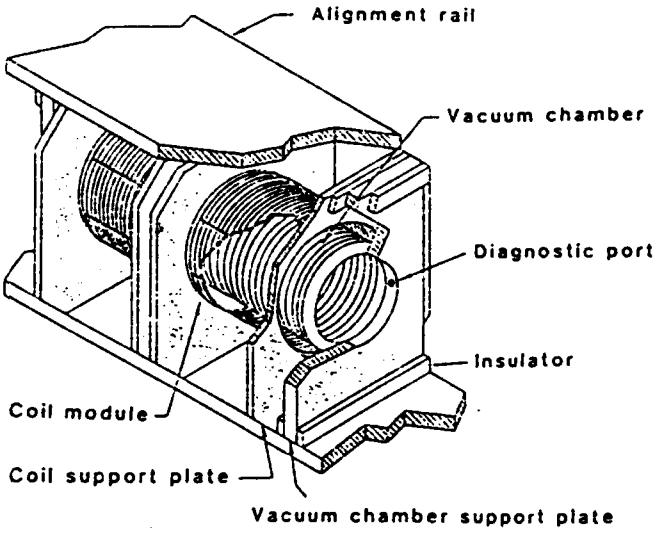

Fig. 2. Construction details of main ring, UNM Betatron.

A number of technical innovations have been incorporated in the UNM Betatron to achieve high energy efficiency and to optimize the versatility of the machine as a research device. Modular construction techniques have been used for all machine systems. For example, the device can be configured either as a racetrack with external injection or as a circular accelerator with an internal electron source. The technology of the main acceleration ring, high voltage injector, and beam inflector are reviewed in the following section. Experimental results on the performance of the injector, and high current transport in a linear periodic system are summarized in Section 3. Section 4 describes measurements of beam transport in a 180° betatron sector. Presently, the machine is set up in a closed circular configuration. Transport of 50 keV electrons around the full circumference has been confirmed. Experiments are currently being performed on the acceleration of runaway electrons from a preionized, cusp contained plasma.

2. Features of the UNM Betatron

The main acceleration ring of the UNM betatron is illustrated in Fig. 1. Inductive isolation is provided by modular toroidal transformer cores. The ten cores are fabricated from 3000 turns of 4 mil silicon steel for fast pulse response. The volt-second product of the cores implies a maximum beam energy of 15 MeV for the 8 m circumference device. The accelerator output energy can be extended to 30 MeV with additional cores. The support system for the cores is mechanically independent of the precision alignment system for the main ring.

Fig. 2 is a detailed view of the main ring. The vacuum chamber consists of 18 stainless steel bellows assemblies with 13 mil wall thickness. The all-metal chamber construction avoids problems of beam space charge induced breakdowns. The vacuum chamber is interrupted by two re-entrant acceleration gaps. The bellows assemblies are supported by rigid plates with two diagnostic ports per plate.

Magnetic fields for beam bending and focusing are applied by 36 coil modules. Each module contains independent solenoidal and vertical field windings with low mutual inductance. The vertical field windings generate a sector field that can rapidly penetrate the thin vacuum chamber wall. The winding geometry was designed for highly uniform horizontal deflection over a 5 cm width. The properties of the fast isolation cores, thin vacuum chamber and sector-type vertical fields are compatible with acceleration cycles as short as 20 microseconds. The modular coils can be connected in various series-parallel combinations to achieve a wide range of risetimes for the focusing and acceleration fields. The coils are designed for applied voltage up to 10 kV.

The main ring components are mounted on 2 m diameter aluminum rails fabricated on a vertical mill. The vacuum chamber supports are isolated from the rails with insulating spacers to force beam return currents through the bellows. Vacuum pumping is performed by an 8" cryopump and an 8" ion pump. Pulsed power for the focusing fields, vertical fields and beam acceleration is supplied by two ignitron controlled 5 kJ capacitor banks. The acceleration bank is sufficient for beam loads to 2 kA. The acceleration cycle of the betatron and injector is computer controlled by a CAMAC system.

A variety of beam formation techniques, both in plasma and high vacuum environments, will be studied. The baseline technique involves trapping of a high energy beam (150 A, 300-600 keV) by pulsed, transverse electric fields. The beam inflector assembly, located in the 1 m racetrack section, is shown in Fig. 3. It consists of a magnetically shielded injection chamber and two 46 cm long electrodes that extend through three focusing cells of the downstream transport tube. The magnitude of the applied electrode voltage is 40 kV. The beam enters through a slot in the positively biased upper electrode. After the beam fills the betatron, the electrodes are rapidly shorted together by a distortion spark gap triggered by a delayed pickoff from the injector voltage. The beam is carried from the HV injector through a 1 meter long, 3.4 cm diameter transport tube with a 25 cell periodic focusing system.

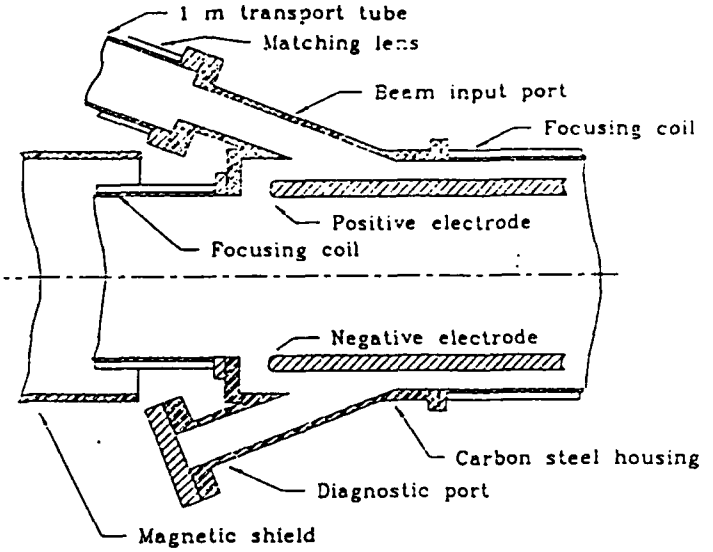

Fig. 3. Inflector assembly

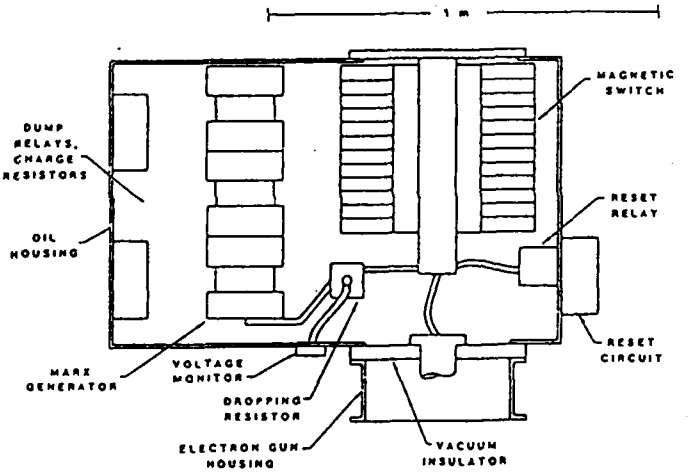

Fig. 4. Injector pulsed power system.

3. Injector experiments

The injector uses the novel pulsed power system illustrated in Fig. 4 to achieve a flat voltage waveform and high operational reliability. The electron gun is driven directly from a 200 kV Marx generator; the gun voltage is crowbarred after 80 ns by a saturable core magnet in the line consisting of 12 fast ferrite cores of 14 cm diameter. The combination of a reliable crowbar and ferrite isolation allows reproducible beam generation with a simple cold surface cathode. The same cathode has been used for over 2000 shots at 1 kA/cm² with no degradation in current output. The [illegible] beam currents up to 1.5 kA with [illegible] risetimes for the injector voltage [illegible] at the end of the 1 m transport tube are shown in Fig. 5. During the next year, the voltage of the injector will be raised to 600 kV by replacing the Marx switch as a 2:1 step-up transformer.

A series of beam propagation experiments were carried out using the injector and the 1 m transport tube. Results are reported in Ref. 6. A 290 A, 2.5 cm diameter beam was produced with a measured brightness of 2.6×10^6 A/(m-rad)^2. The beam was compressed for entry into the 1 m transport tube by a solenoidal lens. A well-directed beam of 150 A was transported through the tube. The polarity of the linear transport tube coils could be changed to generate both cusp fields and a straight solenoidal field. There was little observed difference in beam propagation characteristics for the two field geometries.

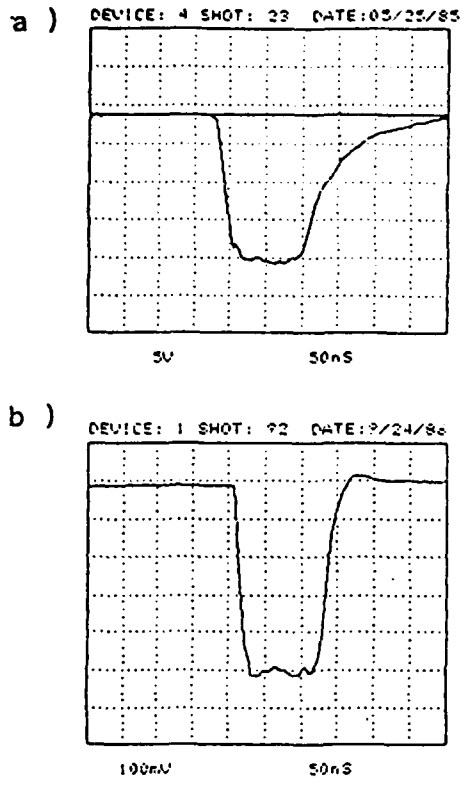

Fig. 5. Injector waveforms. a) Voltage, 70 kV/div, 50 ns/div. b) Current at exit of 3.2 m transport system, 22 A/div, 50 ns/div.

4. 180° sector experiments

A series of measurements on high current beam transport through a 180° sector of the main ring are reported in Ref. 7. The 300 kV beam from the injector was injected directly into the end of the sector. Detailed beam diagnostics could be performed in the open system. The main purpose of the experiments was to verify efficient transport in the 18 cell periodic focusing system and to make a direct comparison between cusp focusing and toroidal field focusing in a curved geometry. The polarity of adjacent focusing field coils was changed while maintaining constant parameters on the injector and matching optics.

As predicted, the periodic focusing system provided excellent containment of a 30 A beam at high vacuum. The rapidly reversing field polarity canceled transverse drift motions. In consequence, beam transport was quite tolerant to vertical field errors and system asymmetries. Fig. 6 indicates that a 100% vertical field error shifted 50% of the beam out of the acceptance of a 5.4 cm diameter current monitor at the downstream end of the transport tube. The optimum vertical field value corresponded to a match between the particle gyroradius and the 1 m radius of the transport system. Observations of the beam distribution at the end of the 3.2 m transport tube showed that field errors resulted in a horizontal shift of the beam centroid with little effect on the beam shape. The magnitude of the displacement was in agreement with theory.

In contrast, beam transport in a monodirectional toroidal field with 50% modulation was dominated by drift motions. Fig. 6 shows that collected beam current was reduced by 50% with only an 8% error. Beam distribution measurements showed that vertical field errors resulted in a distorted beam profile and large vertical displacements. The vertical field value corresponding to optimum beam transport was shifted up 50% compared to the value for cusp transport because of the effect of the grad-B drift. Beam displacements were in qualitative agreement with drift orbit theory. While the beam in the cusp array reached an approximate displacement equilibrium at the end of the transport tube, drift theory predicts that the beam in the toroidal field would suffer further displacement with increased system length. The actual tolerance on beam energy error in the modulated toroidal field is probably in the range 1-2%.

This work was supported by the Office of Naval Research under Contract No. N00014-84K-0248.

References

1. See, for instance, C.A. Kapetanakos, these proceedings.
2. S. Humphries, Jr. and D.M. Woodall, Bull. Am. Phys. Soc. 28, 1054 (1983).
3. H. Ishizuka, G. Leslie, B. Mandelbaum, A. Fisher, and N. Rostoker, IEEE Trans. Nucl. Sci. NS-32, 2727 (1985).
4. J. Golden, J. Pasour, D.E. Pershing, K. Smith, F. Mako, S. Slinker, F. Mora, N. Orick, R. Altes, A. Fliflet, P. Champney and C.A. Kapetanakos, IEEE Trans. Nucl. Sci. NS-30, 2114 (1983).
5. C.W. Roberson, A.A. Mondelli and D. Chernin, Phys. Rev. Lett. 50, 507 (1983).
6. S. Humphries, Jr., L.K. Len and C.B. Allen, to be publishe , Rev. Sci. Instrum.
7. S. Humphries, Jr. and L.K. Len, submitted to J. Appl. Phys.

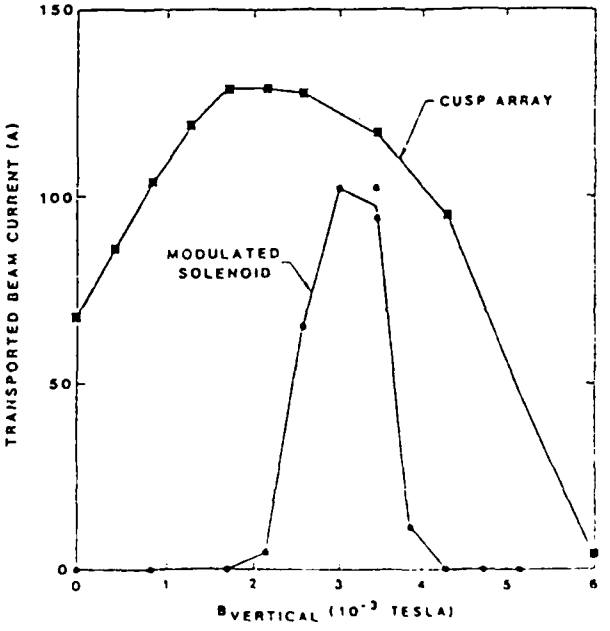

Fig. 6. Beam current detected at downstream end of 180° sector as a function of vertical field. Peak focusing field, 0.05 t.

END

7-87

DTIC